Structure of the 1–36 Amino-Terminal Fragment of Human Phospholamban by Nuclear Magnetic Resonance and Modeling of the Phospholamban Pentamer

Piero Pollesello,* Arto Annila,# and Martti Ovaska*

*Orion Corporation, Orion Pharma, Department of Pharmacology and Drug Discovery, Cardiovascular Research, FIN-02101 Espoo, and #VTT, Chemical Technology, FIN-02044 VTT, Finland

ABSTRACT The structure of a 36-amino-acid-long amino-terminal fragment of phospholamban (phospholamban[1–36]) in aqueous solution containing 30% trifluoroethanol was determined by nuclear magnetic resonance. The peptide, which comprises the cytoplasmic domain and six residues of the transmembrane domain of phospholamban, assumes a conformation characterized by two α-helices connected by a turn. The residues of the turn are Ile18, Glu19, Met20, and Pro21, which are adjacent to the two phosphorylation sites Ser16 and Thr17. The proline is in a *trans* conformation. The helix comprising amino acids 22–36 is well determined (the root mean square deviation for the backbone atoms, calculated for a family of 18 nuclear magnetic resonance structures is 0.57 Å). Recently, two molecular models of the transmembrane domain of phospholamban were proposed in which a symmetric homopentamer is composed of a left-handed coiled coil of α-helices. The two models differ by the relative orientation of the helices. The model proposed by Simmerman et al. (H.K. Simmerman, Y.M. Kobayashi, J.M. Autry, and L.R. Jones, 1996, J. Biol. Chem. 271:5941–5946), in which the coiled coil is stabilized by a leucine-isoleucine zipper, is similar to the transmembrane pentamer structure of the cartilage oligomeric membrane protein determined recently by x-ray (V. Malashkevich, R. Kammerer, V. Efimov, T. Schulthess, and J. Engel, 1996, Science 274:761–765). In the model proposed by Adams et al. (P.D. Adams, I.T. Arkin, D.M. Engelman, and A.T. Brunger, 1995, Nature Struct. Biol. 2:154–162), the helices in the coiled coil have a different relative orientation, i.e., are rotated clockwise by $\sim$50°. It was possible to overlap and connect the structure of phospholamban[1–36] derived in the present study to the two transmembrane pentamer models proposed. In this way two models of the whole phospholamban in its pentameric form were generated. When our structure was connected to the leucine-isoleucine zipper model, the inner side of the cytoplasmic domain of the pentamer (where the helices face one another) was lined by polar residues (Gln23, Gln26, and Asn30), whereas the five Arg25 side chains were on the outer side. On the contrary, when our structure was connected to the other transmembrane model, in the inner side of the cytoplasmic domain of the pentamer, the five Arg25 residues formed a highly charged cluster.

INTRODUCTION

Phospholamban (PLB)[1] is a low molecular weight protein (52 amino acids), present in cardiac, slow-twitch, and smooth muscle, which can be phosphorylated by both cAMP-dependent (Karczewski et al., 1987) and Ca^{2+}/calmodulin-dependent (Iwasa et al., 1985) phosphokinases. The phosphorylation/dephosphorylation of phospholamban has been shown to regulate the Ca^{2+}-ATPase of the sarcoplasmic/endoplasmic reticulum in myocytes (SERCA2) (Tada and Kadoma, 1989; Jackson and Colyer, 1996). Phospholamban, in its nonphosphorylated form, binds to a specific region of the large loop in the cytoplasmic domain of SERCA2 and inhibits this pump by lowering its affinity for Ca^{2+}, whereas the phosphorylated form does not inhibit SERCA2 (Toyofuku et al., 1993).

It has been proposed that a region essential for functional association of phospholamban with Ca^{2+}-ATPase lies in the cytoplasmic domain of phospholamban (Sasaki et al., 1992; Hughes et al., 1994a; Toyofuku et al., 1994a), whereas the transmembrane region anchors PLB to the sarcoplasmic membrane (Sasaki et al., 1992). However, it has been recently proposed that the transmembrane region may also exert an effect on SERCA2 (Kimura et al., 1996; Starling et al., 1996). Moreover, evidence has been given that the transmembrane domain of PLB induces the formation of a PLB pentamer (Imagawa et al., 1986; Fujii et al., 1989), which was also proposed to be a calcium ion pore (Kovacs et al., 1988).

During the last decade, the objective has been to elucidate, at least partially, the secondary structure of PLB either indirectly by means of cross-linking experiments and by reconstitution or co-expression of SERCA2 with point-mutated PLB (Jones and Field, 1993; Meyer et al., 1995; Hughes et al., 1996; Simmerman et al., 1996) or directly by circular dichroism (CD) (Simmerman et al., 1989; Terzi et al., 1992; Vorherr et al., 1992), laser-light-scattering photometry Fourier transform infrared (FTIR) spectroscopy (Tatulian et al., 1995; Ludlam et al., 1996), and nuclear magnetic resonance (NMR) spectroscopy (Gao et al., 1992; Hubbard et al., 1994; Maslennikov et al., 1995; Mortishire-Smith et al., 1995; Quirk et al., 1996).

As PLB is an amphiphatic oligopeptide, contains three cysteins, and is prone to pentamerization also in vitro (Sim-

Received for publication 17 April 1998 and in final form 9 January 1999.

Address reprint requests to Dr. Piero Pollesello, Orion Corporation, Orion Pharma, Department of Pharmacology and Drug Discovery, Cardiovascular Research, P.O. Box 65, FIN-02101 Espoo, Finland. Tel.: 358-9-429-4191; Fax: 358-9-429-2924; E-mail: piero.pollesello@orion.fi.

0006-3495/99/04/1784/12 $2.00

merman et al., 1986), it is not trivial to find experimental conditions to study its structure and, in particular, an appropriate solvent system that prevents nonspecific aggregation. Therefore, until now NMR studies have been carried out either on short PLB fragments (Gao et al., 1992; Hubbard et al., 1994; Mortishire-Smith et al., 1995; Quirk et al., 1996) or in organic solvents (Maslennikov et al., 1995). In no cases is there evidence of a tertiary structure for the cytoplasmic domain of PLB. The present investigation aims to assess the secondary and tertiary structure of a 36-amino-acid-long fragment of phospholamban, which comprises the cytoplasmic domain and six amino acids of the transmembrane domain, in an aqueous solution.

Recently, molecular modeling and mutagenesis studies have been used to formulate hypotheses on the quaternary structure of the transmembrane region in the PLB pentamer, and two models were proposed, which both show a left-handed coiled coil (Adams et al., 1995; Simmerman et al., 1996). The two models, however, differ by the relative orientation of the five helices, and although in the model proposed by Simmerman et al. the coiled coil is stabilized by a leucine-isoleucine zipper (Simmerman et al., 1996; Karim et al., 1998), in the model proposed by Adams et al., different heptad positions are packed together due to a rotation of ~50° of the helices (Adams et al., 1995). There are no direct structural data supporting either of these models. However, the structure of another transmembrane pentamer, the cartilage oligomeric membrane protein (COMP), was recently determined by x-ray crystallography (Malashkevich et al., 1996), and the quaternary structure of the five oligomers is fully consistent with the leucine-isoleucine zipper model of PLB.

It was possible to overlap and connect the structure of phospholamban[1–36] derived in the present study to both of the PLB transmembrane pentamer models proposed. In this way two models of the whole phospholamban in its pentameric form were generated and their structure discussed.

MATERIALS AND METHODS

Peptide synthesis and purification

The 36-amino-acid amino-terminal fragment of human PLB (PLB[1–36]) was obtained by peptide synthesis by using the method described by Vorherr et al. (1993). The peptide was purified by reverse phase high-pressure liquid chromatography and analyzed for homogeneity by mass spectrometry and SDS-polyacrylamide gel electrophoresis.

CD spectra were acquired at 24°C on a sample of 3 μM PLB[1–36] in H_2O:D_2O:perdeuterated trifluoroethanol (d_3-TFE; 63:7:30) containing 6 μM perdeuterated dithiothreitol (d_{10}-DTT) at pH 3.05 ± 0.05 (the pH value is uncorrected for the deuterium effects). The spectra were recorded on a Jasco J-720 spectropolarimeter using a 1-mm path-length quartz cuvette. The band width was 1 nm, the sensitivity 20 mdeg, the step resolution 0.5 nm, the response time 0.5 s, and the scan speed 20 nm/min (from 270 to 190 nm). In the spectra, expressed in $[\theta] \times 10^{-3} \times$ degrees $\times$ cm^2 $\times$ dmol^{-1}, a contribution of α-helix structure of 80% was calculated from the local minimum at 220 nm.

NMR spectra

^{1}H-NMR spectra were acquired at 400.13 MHz and at 599.86 MHz on a Bruker ARX400 and a Varian UNITY 600 NMR spectrometer, respectively. One- and two-dimensional NMR spectra were obtained for a 3 mM solution of the 36-amino-acid fragment of PLB in the solvent mixture H_2O:D_2O:d_3-TFE (63:7:30) containing 6 mM d_{10}-DTT to prevent disulfide formation. The pH was adjusted to 3.05 ± 0.05 (uncorrected for deuterium isotope effects) with microliter amounts of NaOD. Correlation spectroscopy (COSY) (Aue et al., 1976), total COSY (TOCSY) (Braunschweiler and Ernst, 1983), and nuclear Overhauser-enhancement spectroscopy (NOESY) (Kumar et al., 1980) (40–400 ms) spectra were recorded at 2°C, 7°C, 17°C, and 27°C, by the States-TPPI method (Marion et al., 1989b), using a spectral width of 8.5 ppm. The two-dimensional data were weighted and Fourier transformed to 2000 × 1000 real-point matrices. The transmitter presaturated (2.0 s) residual solvent line was reduced by a convolution difference filter technique (Marion et al., 1989a). The spectra were referenced to the residual solvent signal (4.75 ppm at 27°C, −10 ppb/°C). A series of 10 one-dimensional spectra was acquired at different temperatures from 2°C to 47°C.

Assignment of the NMR spectra

The spin-system and sequential assignments were derived from COSY, TOCSY, and NOESY spectra (Wüthrich, 1986), acquired at 12°C, 17°C, and 27°C. Differences in the temperature dependencies of the amido proton chemical shifts were sufficient to unravel resonance overlap. Stereospecific assignments for nondegenerated methylenes were deduced from coupling constants $J_{H\alpha H\beta}$ measured from the COSY spectra and from intra-residual NOE cross-peak intensities (Chazin et al., 1988).

Structure generation and refinement

A series of NOESY spectra was acquired at 17°C with five different mixing times (50, 80, 120, 160, and 200 ms). The integrated cross-peak intensities (I) were used in a NOESY-built-up analysis. Distance restraints were extracted from the initial slope of a second-order polynomial curve fitted to the volumes of the cross-peaks integrated from the NOE series, with the initial condition $I_{(\tau m=0)} = 0$. Intra-methylene and sequential NOEs served for the calibration. The distances were initially classified as short (1.8–2.5 Å), medium (1.8–3.5 Å), or long (3.0–6.0 Å) for the generation of the first set of structures. When a distance could not be calculated from the built-up curve, owing to a partial (>20%) overlap, a poor signal-to-noise ratio, or disturbances, it was required only that the distance was <5.0 Å. The upper bounds were extended by 1.0 Å for each pseudo-atom. The restraint data were supplemented with distance restraints, which were based on strong, medium, and weak NOEs, from the 150-ms NOE spectrum acquired at 12°C. In the segments characterized by NOEs typical of α-helices, the Hα-chemical shift of consequent residues departed from the corresponding random coil value more than −0.2 ppm, which also implies α-helical values for the ϕ and ψ dihedral angles (Wishart et al., 1991a,b). Small δ_{NH} (T) values suggested also that NH tends to form hydrogen bonds most likely with backbone carbonyls in the same helix.

Coupling constants (J) were measured by the J-doubling method (McIntyre and Freeman, 1992) from fine structures of COSY cross-peaks. Dihedrals ϕ and χ, which were characterized by intermediate J values, were not constrained, but small and large $J_{NH\alpha}$ and $J_{H\alpha H\beta}$ were related to staggered conformers (±30°) on the basis of Karplus functions and intra-residual NOEs (Karplus, 1963). The H-H distance and dihedral angle restraints were calculated with the software FELIX (Molecular Simulations). Finally, the data were imported into the software InsightII (Molecular Simulations, San Diego, CA) to generate and refine the structures. Simulated NOESY spectra were back calculated. The family of protein structures was analyzed by the software Procheck nmr v.3.4.4 (Laskowski et al., 1996).

Structures were generated by distance geometry (DGII) followed by simulated annealing (force field AMBER) (Havel et al., 1979). A set of 100

structures was computed. Among them, 18 structures with no violations over 0.2 Å were accepted.

The distance restraints corresponding to well resolved cross-peaks were refined by an iterative relaxation matrix method (IRMA) based on a structure without restraint violations (>0.2 Å, >0°) (Boelens et al., 1988). The upper bounds were kept within at least 10% of the exact distance given by IRMA to take into account the uncertainty in correlation time τ_c. The refined restraint set was subsequently used to refine the coordinates by simulated annealing (Brünger et al., 1986).

Modeling of the pentamer

To create models for the whole PLB[1–52], the structure of PLB[1–36] was overlapped and connected to both transmembrane pentamer models previously proposed. A similar approach has been recently used to connect the structure of the cytoplasmic loops of bovine rhodopsin on the transmembrane α-helices, whose structures were determined separately and with other techniques (Yeagle et al., 1997).

Two models for the packing of the transmembrane domain of PLB in a pentamer structure have been proposed (Adams et al., 1995; Simmerman et al., 1996). The two models agree on two points, namely, 1) that the transmembrane region (amino acids 30–52) is a symmetric homopentamer in which the five monomers are coordinated in a left-handed coiled coil of α-helices and 2) that there is not any deviation from the α-helical secondary structure throughout the transmembrane region. The two models differ for the relative orientation of the five helices and for the amino acids involved in the interhelical zippers that stabilize the pentamers. We will refer to the model proposed by Simmerman et al. (1996) by the leucine-isoleucine zipper model because the complex is stabilized by interactions between leucines at one heptad position with isoleucines at another. This packing is supported by the x-ray structure of the cartilage oligomeric matrix protein (COMP) (Malashkevich et al., 1996) with similar heptad assignments. The model proposed by Adams et al. (1995) differs from the leucine-isoleucine zipper model so that each helix in the pentamer is rotated clockwise by ~50°, thus leading to quite different contacts between the helices. Both the coordinates of the model by Adams et al. and those of COMP, analogous to the leucine-isoleucine zipper, are available from the Brookhaven Protein Databank (structures 1psl and 1vdf, respectively) (Bernstein et al., 1977).

PLB[1–36] was connected on the transmembrane leucine-isoleucine zipper model (1vdf) as follows. The α-carbon atoms of the residues Gln22-Cys36 in the structure of PLB[1–36] were superimposed to the α-carbon atoms of the residues Ala30-Ala43 of 1vdf, according to the heptad sequence alignment (Malashkevich et al., 1996). The two proteins were fused so that Asn30 of PLB[1–36] was connected to Gln38 of 1vdf. The unconnected parts were deleted and the carboxy terminal of 1vdf truncated at Thr59 (residue that corresponds to Leu52 of PLB). Finally, the side chains in the 1vdf structure were substituted by the corresponding side chains of PLB. The derived pentamer model of PLB was refined by simple energy minimization. The same protocol was also used to overlap and connect the structure of PLB[1–36] on the transmembrane model proposed by Adams et al., starting from the Brookhaven protein database file 1psl (Bernstein et al., 1977).

All of the 18 NMR structures of PLB[1–36] with no violations over 0.2 Å could be connected to both transmembrane models as described above. However, as the experimental root mean square deviation (rmsd) of the backbone in the region 22–36 was below 0.6 Å, for the sake of clarity, some of the figures illustrate only the models obtained from the structure of PLB[1–36] with the least NOE violations. All molecular modeling was done by the InsightII software (Molecular Simulations).

RESULTS

Assignment

The complete spin-system and sequential assignments were obtained under the experimental conditions described. The assignments are listed in Table 1. In addition to the cross-peaks arising from PLB[1–36], several cross-peaks were observed that may arise either from peptide impurities (<5%) or from conformational isomers. No effort was made to assign these correlations because there were no connections from the minor peaks to the main peaks.

PLB[1–36] spectra displayed chemical shift dispersion over 8.5 ppm. Predominantly, $C_\alpha H$ shifts were at high field as expected on the basis of the CD measurements. However, the $\delta_{C\alpha H}$ of the residues at the amino and carboxy termini as well as for Glu19, Met20, and Pro21 were not shifted at high field. Most NH shifts were confined within 1.5 ppm, but for Glu2, Lys3, Val4 and Leu7, Gln22, and Gln23 the NH resonances were shifted down-field. There were no signals of methyl groups at very high field (≤0 ppm).

In total, 724 NOEs were assigned. All of the 34 possible intra NH-$C_\alpha H$ correlations were observed in the fingerprint region. Most of the corresponding NOEs were fairly strong and comparable to sequential NH_{i+1}-$C_\alpha H_i$ NOEs (Fig. 1). Many sequential NH_i-NH_{i+1} and NH_i-NH_{i+2} NOEs were present. Numerous $C_\alpha H_i$-NH_{i+3} and some $C_\alpha H_i$-NH_{i+4} NOEs were crowded in the fingerprint region of the NOESY spectra (Fig. 2 *A*). Furthermore, there were a number of $C_\alpha H_i$-$C_\beta H_{i+3}$ cross-peaks. NOEs derived from interactions longer than $i > i + 4$ were observed only for protons of Met20.

J-couplings between NH and $C_\alpha H$ were small for most residues. Due to overlap of resonances or weak intensity of COSY cross-peaks it was not possible to measure accurate values for all residues, but the couplings were below 6–7 Hz with the exception of the residues at the amino and carboxy termini and in the center of PLB[1–36].

The high-field $\delta_{C\alpha H}$, the NOE values, and the small $J_{NH\text{-}C\alpha H}$ values imply that residues Lys3-Ile18 and Gln22-Phe35 are in an α-helical structure. For the amino- and carboxyl-terminal residues, the NMR data were not as abundant as for the other residues, but nevertheless, the helices extend to the termini as well (Fig. 1). A number of significant i, $i + 3$ and i, $i + 4$ NOEs indicate a well defined structure at the carboxy terminus.

On the contrary, the central region of the PLB[1–36] does not show a helical character. Namely, the $\delta_{C\alpha H}$ values of the residues Glu19, Met20, and Pro21 were not significantly smaller than their random coil values. Glu19 and Met20 were mostly devoid of the NOEs typical of a helical structure, and there were unambiguous strong sequential NOEs between $C_\alpha H$ of Glu19 and NH of Met20 and between $C_\alpha H$ of Met20 and $C_\delta Hs$ of Pro21 (Fig. 2, *A* and *B*). Furthermore, the NOE between $C_\alpha H$ of Ile18 and NH of Glu19 is strong. All this implies that the central region of PLB[1–36] assumes an extended-like conformation. The extended segment is, nevertheless, short. Thr17 and Gln22 show NOEs and coupling constants characteristic of residues in an α-helix, and there are NOEs from the side chain protons of Glu19 and Met20 to the protons of the adjacent residues in the amino- and carboxyl-terminal helices. We conclude that the amino- and carboxyl-terminal α-helices are separated by

TABLE 1 H-chemical shifts of PLB[1–36] in 63% H_2O/7% D_2O/30% d_3-TFE, pH 3.05, at 17°C

Residue	NH	$C_\alpha H$	$C_\beta H$	$C_\gamma H$	$C_\delta H$	Others
Met1		4.159	2.124	2.566		2.012
Glu2	8.803	4.572	1.967	2.510, 2.319		
Lys3	8.787	4.147	1.900	1.559, 1.431	1.729	2.969
Val4	8.314	3.889	2.132	1.026, 0.951		
Gln5	7.846	4.092	2.364, 2.252	2.369		7.431, 6.823
Tyr6	7.924	4.225	3.114		7.046	6.780
Leu7	8.536	4.013	1.831	1.586	0.915	
Thr8	7.975	3.955	4.247	1.222		
Arg9	8.156	3.518	1.845, 1.725	1.587	3.092	7.242
Ser10	7.991	4.082	3.936, 3.767			
Ala11	8.051	4.085	1.510			
Ile12	8.126	3.681	1.857	1.704, 1.014	0.769	0.860
Arg13	8.181	3.983	1.941, 1.735	1.606	3.162	7.189
Arg14	8.143	4.052	1.941, 1.733	1.725, 1.604	3.169	7.154
Ala15	8.422	4.114	1.500			
Ser16	8.110	4.275	4.029, 3.979			
Thr17	7.695	4.316	4.373	1.270		
Ile18	7.589	4.102	1.925	1.576, 1.216	0.851	0.912
Glu19	8.149	4.351	2.121, 2.011	2.468, 2.426		
Met20	7.958	4.702	2.088	2.544		2.027
Pro21		4.487	2.539, 2.483	2.082, 1.948	3.876, 3.591	
Gln22	8.766	4.008	2.173	2.438		7.433, 6.742
Gln23	8.954	4.079	2.084, 1945	2.464		7.457, 6.784
Ala24	7.455	4.155	1.474			
Arg25	7.858	3.944	1.876, 1712	1.604	3.246, 3.181	7.253
Gln26	8.143	4.019	2.136, 2.115	2.461, 2.374		7.371, 6.721
Lys27	7.647	4.069	1.954, 1.598	1.613, 1.465	1.682	2.937, 7.604
Leu28	8.099	4.063	1.773, 1.712	1.510	0.849, 0.818	
Gln29	8.212	3.985	2.198, 2.117	2.480, 2.367		7.172, 6.668
Asn30	7.908	4.482	2.884, 2.803		7.486, 6.821	
Leu31	7.878	4.154	1.718, 1.625	1.557	0.859, 0.797	
Phe32	8.162	4.430	3.238, 3.096		7.173	7.197
Ile33	7.974	3.986	1.930	1.611, 1.283	0.900	0.891
Asn34	7.801	4.570	2.588, 2.511		7.337, 6.759	
Phe35	8.006	4.694	3.272, 3.058		7.277	7.207
Cys36	7.727	4.452	2.890			

The staggered conformations are denoted by a line under the chemical shift of $C_\beta H$ if they had been proven to be in an anti-configuration to $C_\alpha H$.

a turn at Ile18, Glu19, Met20, and Pro21. The proline is in a *trans* conformation. A tight turn, which would result the axes of the amino- and carboxyl-terminal helices being parallel, is not possible. There were no unambiguous NOEs between the amino- and carboxyl-terminal helices.

The study of the temperature dependence of NH chemical shifts shows that most residues with high-field $\delta_{C\alpha H}$ have small $\Delta\delta_{NH}$ (T) compared with the temperature dependence of the water line (not shown). This suggests that these NH are hydrogen bonded with backbone CO with the exception of the amino-terminal residues Glu2, Lys3, and Val4, which move with temperature. For these residues at the amino terminus there are, of course, no α-helical hydrogen bond acceptors. We find no evidence for an end capping either. It is difficult on the basis of the NOEs to unambiguously distinguish between α-helix and 3_{10}-helix (Wüthrich, 1986) as the acceptor oxygens cannot be identified by NMR data (Halkides and Redfiels, 1995), but we observed certain $C_\alpha H_i$-NH_{i+4}, which imply the α-helical structure.

In the carboxyl-terminal helix, the NH frequencies of Gln22 and Gln23 clearly move with the temperature. The NH shift of Arg25 has only small temperature dependence; a possible hydrogen bond acceptor may in fact be the oxygen of the peptide bond Pro21-Gln22. This is further proof that the helical structure begins at Gln22.

In the middle of the two α-helices, Leu7, Phe32, and Ile33 have larger $\Delta\delta_{NH}$ (T) than the other residues. This apparent anomaly may be explained in light of the recent finding (Rothemund et al., 1996) that large chemical shift temperature dependences are observed for some of the amide protons in an α-helix in the presence of TFE, possibly due to intramolecular hydrogen bonds between TFE and the peptic carbonyl groups. This interaction depends on solvent accessibility and thus also on steric hindrance of the side chains.

Also, the NH of Ile18, Glu19, and Met20 have only modest temperature dependence. This implies that there is a well defined turn, possibly with hydrogen bonds, or that those NH are buried and not accessible to the solvent (Baxter and Williamson, 1997). The side chain ϵNH shifts of Arg9, Arg13, and Arg14 are practically independent of temperature, whereas $\Delta\delta_{\epsilon NH}$ (T) of Arg25 is comparable to

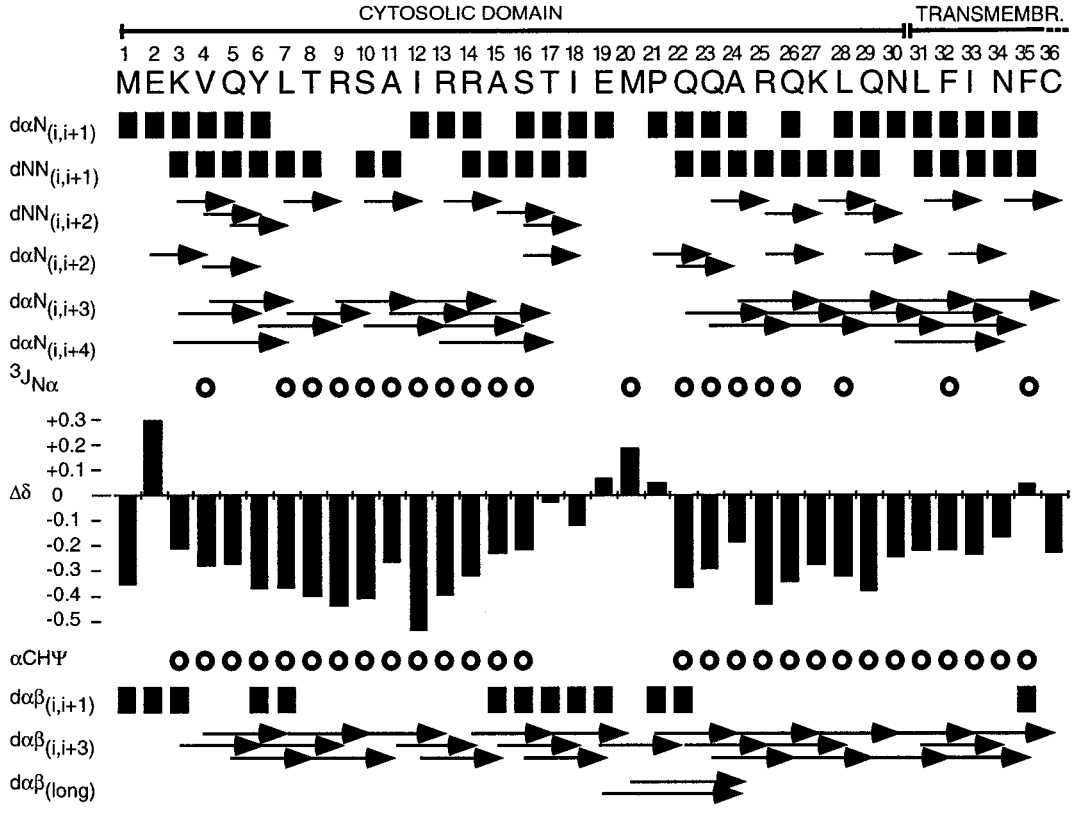

FIGURE 1 Summary of observed sequential and medium-range NOE connectivities for PLB[1–36] in 63% H_2O/7% D_2O/30% d_3-TFE, pH 3.05, at 17°C from NOESY spectra acquired at 120-, 160, and 200-ms mixing times. Sequential NOEs are represented by shaded blocks. Medium-range NOEs are represented by arrows connecting the appropriate residues. Open circles denote $^3J_{NH\alpha CH}$ coupling constants smaller than 6 Hz. The secondary shift ($\Delta\delta$) of CαH is defined as the difference between the observed chemical shift and the random coil chemical shift for each residue (Wüthrich et al., 1983; Wüthrich, 1986). Negative (upfield) $\Delta\delta$ values are associated with α-helical secondary structure and positive (downfield) $\Delta\delta$ values with β-structure (Wishart et al., 1992).

that of water. Frequencies of glutamine and asparagine side-chain NH_2 have temperature dependences that are only half of that of water. Based on the pitch of the α-helix there are, according to the secondary structure alone, many potential hydrogen bond acceptors in the side chains both in the amino- and carboxyl-terminal helices that may temporally take part in hydrogen bonds and result in moderate temperature dependences for the NH_2 shifts.

We followed also the temperature effect on the protons HH of the four arginine residues; two peaks are resolved at

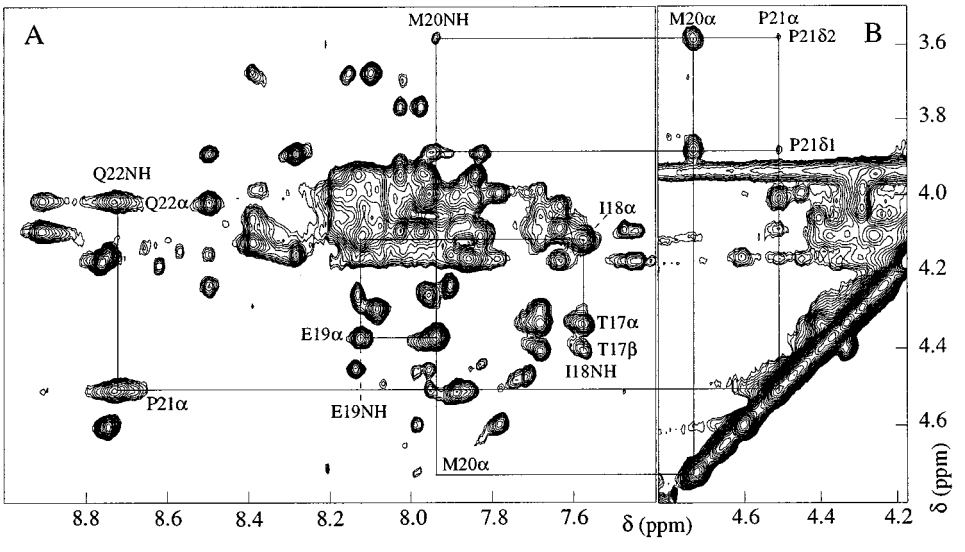

FIGURE 2 Expansions from NOESY spectra acquired at 17°C at 160-ms mixing times on 3 mM PLB[1–36] in 63% H_2O/7% D_2O/30% d_3-TFE, pH 3.05, in the presence of 6 mM d_{10}-DTT. (*A*) Fingerprint region. The cross-peaks generated by the correlations $NH_iC\alpha H_i$ are marked. (*B*) Region showing cross-peaks from the turn Glu19, Met20, Pro21.

2°C, which then coalesce and become one sharp peak at 47°C. The fact that no anomalies are observed from this classical behavior suggests that no strong hydrogen bonds are formed by the terminal protons of arginines in PLB[1–36].

Structure of PLB[1–36]

The structure of PLB[1–36] was determined from 599 distances and 50 dihedral restraints, excluding those that were defined more accurately by the covalent structure alone. These redundant NOE-derived restraints were consistent with the covalently imposed distance limits, which indicated that the calibration of distances was reasonable. On the average there were 16.6 nontrivial NOE-derived restraints per residue. The residues Lys3-Ile18 of the amino-terminal helix had on the average a few restraints fewer per residue than the residues Gln22-Cys36 in the carboxyl-terminal helix. This is at least partly due to the fact that there were on average more protons with nondegenerated shifts per residue in the carboxyl-terminal helix than in the amino-terminal helix (Table 1). For the residues Ile18-Pro21, which confine the turn, there were about as many restraints per residue as there were for the residues in the amino-terminal helix.

The structure generation resulted in a family of structures all of which show two α-helices connected by a turn. The rmsd was computed from the family of 18 structures with no distance violations above 0.2 Å and no dihedral violations (Fig. 3). The small distance restraint violations occurred primarily among the side-chain groups, e.g., methyls and amines. This may be a result of excessive mobility in these parts, which could give rise to nonsimultaneous NOEs.

The mutual orientation of the helices was constrained only by the short-range distance restraints in the turn. Therefore, rmsd per residue was computed separately 1) for the amino-terminal helix (amino acids 1–17) and 2) for the carboxyl-terminal helix (22–36). The rmsd represented roughly an inverse correlation with the number of restraints per residue, as expected (Fig. 3). On the average, the atoms in the amino-terminal helix were defined to a precision of 0.9 Å (backbone only) and of 2.1 Å (all atoms) and in the carboxyl-terminal helix to a precision of 0.6 Å (backbone only) and of 1.6 Å (all atoms) (Table 2). When the hydrogen bond restraints were not imposed, NH_{i+4} and CO_i were predominantly coordinated so that hydrogen bonds can form. This gives the rationale for the weak temperature dependence of the NH chemical shifts for Thr8-Ile18 and Arg25-Leu31. Accordingly, the comparatively large δ_{NH} (T) for Glu2-Val4 as well as for Gln22 and Gln23 are due to the fact that for these residues at the beginning of amino- and carboxyl-terminal helices there are no suitable hydrogen bond acceptors in the backbone. Quite unusual is the large and positive $\Delta\delta_{NH}$ (T) of Ala24 as it cannot find a hydrogen bond donor from the backbone. However, according to the structure, it is possible that the NH of Ala24 forms a hydrogen bond with the side-chain CO of Gln23. Alternately, the δ_{NH} of Ala24 is shielded in the proximity of the side chain of Pro21, which is tilted toward Ala24 above the axis of the carboxyl-terminal helix.

The turn is confined within four residues: Ile18, Glu19, Met20, and Pro21. Despite the number of restraints found in that region, there is a structural dispersion owing to imprecision of the short distance restraints. The smallest number of distance violations (below 0.2 Å) were observed for

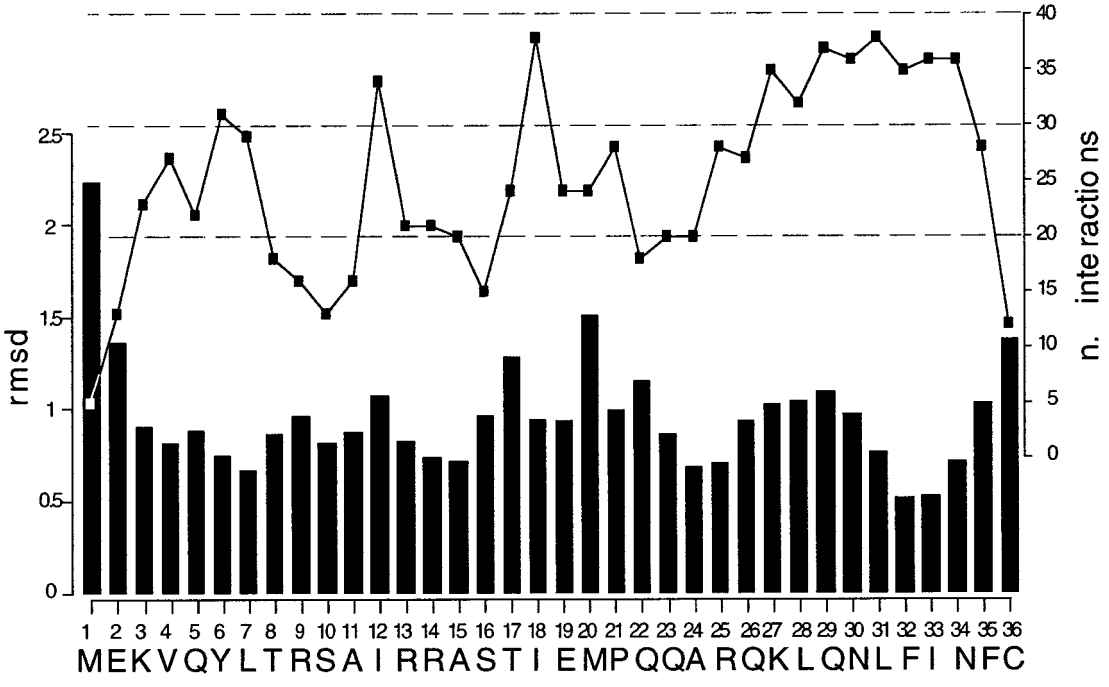

FIGURE 3 Quality of the structure of PLB[1–36] obtained by NOE data: rmsd per residue and number of restraints per residue

TABLE 2 Characteristics of the structures of PLB[1–36]

Parameter	Value
Distance restraints	
Total	724
Short-range	385
Medium-range ($i + 4$)	333
Long-range ($>i + 4$)	6
Dihedral restraints	32
Restraint violations/structure	
Distance of >0.5 Å	0.1
Distance of >0.3 Å	2.4
Distance of >0.1 Å	26.5
rmsd (Å) for region 1–17	
Backbone atoms	0.93 ± 0.22
All atoms	2.09 ± 0.26
rmsd (Å) for region 22–36	
Backbone atoms	0.57 ± 0.12
All atoms	1.62 ± 0.14
ϕ and ψ in core or allowed	97%

Data were computed from a family of 18 structures selected on the basis of the analysis by PROCHECK-NMR (Laskowski et al., 1996).

structures in which the segment from Cα of Glu19 to Cα of Pro21 is extended, the side chain of Met20 protrudes approximately parallel to the carboxyl-terminal helix, and the side chain of Glu19 points almost in the opposite direction. In these structures, the plane of the peptide bond Ile18-Glu19 is nearly orthogonal to the plane of the extended segment.

Owing to the structural imprecision in the turn, the family of structures displays a dispersion in the relative position of the amino- and carboxyl-terminal helices. The dispersion is, nevertheless, limited. When the different structures of the family are superimposed on the Cα of the residues in the carboxyl-terminal helix, the amino-terminal helix is dispersed in a cone with an opening of approximately 80° (Fig. 4). The interhelix angle is 80 ± 20° ($n = 18$). Similar mutual orientations for two sequential helices, one of which is transmembrane and the other amphipathic, have been found or suggested for many small membrane-bound proteins or peptides (Stopar et al., 1996).

In some of the structures, the side-chain ϵNH of Arg9, Arg13, and Arg14, whose chemical shifts are nearly independent of T, make hydrogen bonds with the adjacent side-chain oxygen of Ser10, Ser16, and Thr17. For Arg25, with large $\Delta\delta_{NH}$ (T), there were no obvious candidates for hydrogen bond donors. The side-chain NH_2 of the glutamines and asparagines could form hydrogen bond networks parallel to the helical axis.

With regard to the phosphorylation of PLB, we find important that the phosphorylation site Ser16 is readily accessible and exposed to the solvent. Thr17, on the amino-terminal helix, is facing the carboxyl-terminal helix and appears less exposed to the solvent than Ser16. Due to the pitch of the α-helix, Arg13 and Arg14 are also exposed with orientations that lag 60° in phase with respect to Ser16 and Thr17 on the same side of the helix.

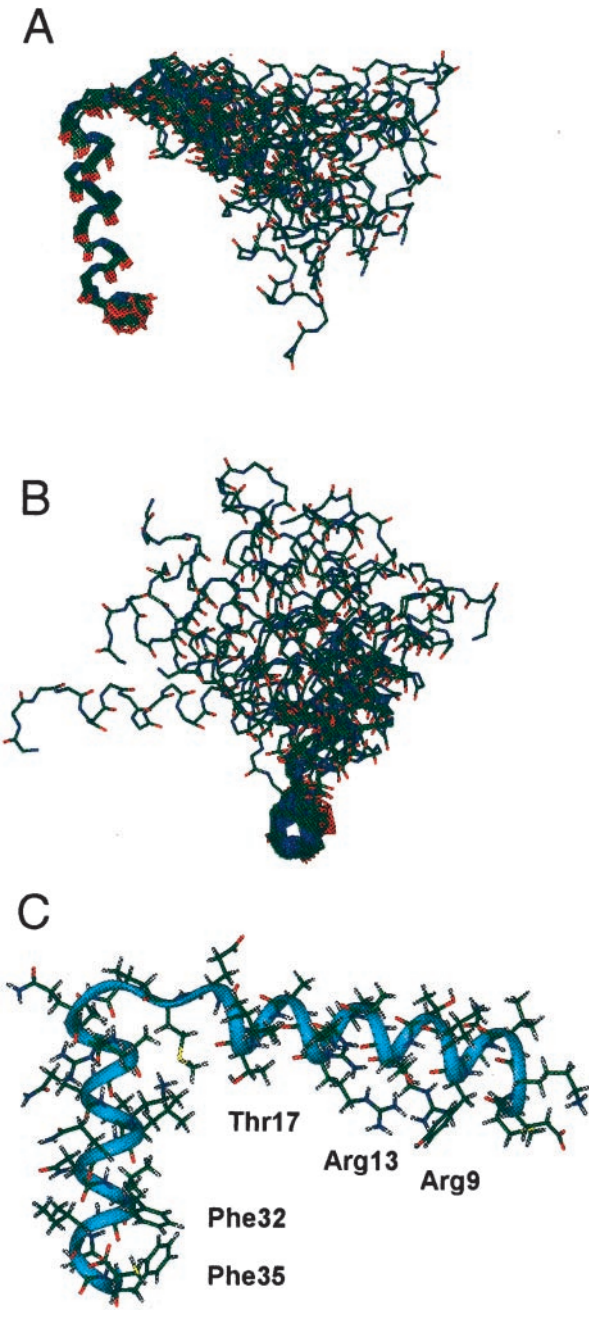

FIGURE 4 Structures of PLB[1–36] deduced from NMR data. (*A* and *B*) Orthogonal view of 18 structures with no violations >0.2 Å, superimposed on the Cα of the residues in the carboxyl-terminal helix. The amino-terminal helix is dispersed in a cone with an opening of approximately 80°. The interhelix angle is 80 ± 20° ($n = 18$). (*C*) The structure with least NOE violations (three violations >0.1 Å, no violations >0.2 Å). Some of the side chains are marked.

Model of the PLB pentamer

The structure of PLB[1–36] proposed in this paper has strong α-helix characteristics throughout the amino acid 22–36 region (see Table 2). On the other side, both of the models proposed in literature for the packing of the transmembrane domain of PLB in a pentamer structure agree that there is not any deviation from the α-helical secondary

structure throughout the transmembrane region (amino acids 30–52). With this rationale, we overlapped and connected our structure to the transmembrane models by using the common region (amino acids 30–36, α-helical both in the 36-mer and in the transmembrane models) as a handle as described in Materials and Methods. In both of the resulting models of the whole PLB[1–52] the α-helices continue unperturbed from Gln22 to Leu52 (Fig. 5).

In our NMR structure of PLB[1–36], despite a structural imprecision in the turn (amino acids 18–21), the family of structures displays a limited angular dispersion in the relative position of the amino- and carboxyl-terminal helices (see Fig. 4, *A* and *B*). Such structures could be easily connected with both of the transmembrane models proposed in the literature; in both cases, in fact, the amino-terminal helices are directed toward the outer perimeter of the pentamer (as shown in Fig. 5). It can be observed that in the pentamer based on the leucine-isoleucine zipper model the cytoplasmic part of the pore (from amino acids 22 to 30) is exclusively lined by polar residues (Gln 22, Gln23, Gln26, and Asn30), which can form a net of H bonds (Fig. 5 *E*) although no steric or electrostatic overlapping occurs. Moreover, every Arg25 is facing toward the outer perimeter (Fig. 5 *C*). In the other case, when the PLB[1–52] pentamer model was obtained by using the model of Adams et al. as a scaffold, the inner side of the cytoplasmic part shows five residues of Arg25 that face one another, thus forming a highly charged cluster (Fig. 5 *D*).

In both models, there is not any evidence for a preferred structure in which the amino-terminal helices assume a constrained position relative to the carboxy termini, and every monomer maintains its flexibility near the turn (amino acids 18–21).

DISCUSSION

The role of PLB in the regulation of SERCA was known (Katz et al., 1975; Kirchberger et al., 1975; Hicks et al., 1979) well before its primary structure was deduced a decade ago from the amino acid (Simmerman et al., 1986) and DNA (Fujii et al., 1987) sequences. However, both the mechanism by which PLB inhibits SERCA and whether PLB may have other physiological roles in the regulation of Ca^{2+} sequestration in cardiac sarcoplasmic reticulum (SR) remain under debate. Moreover, also the relative physiolog-

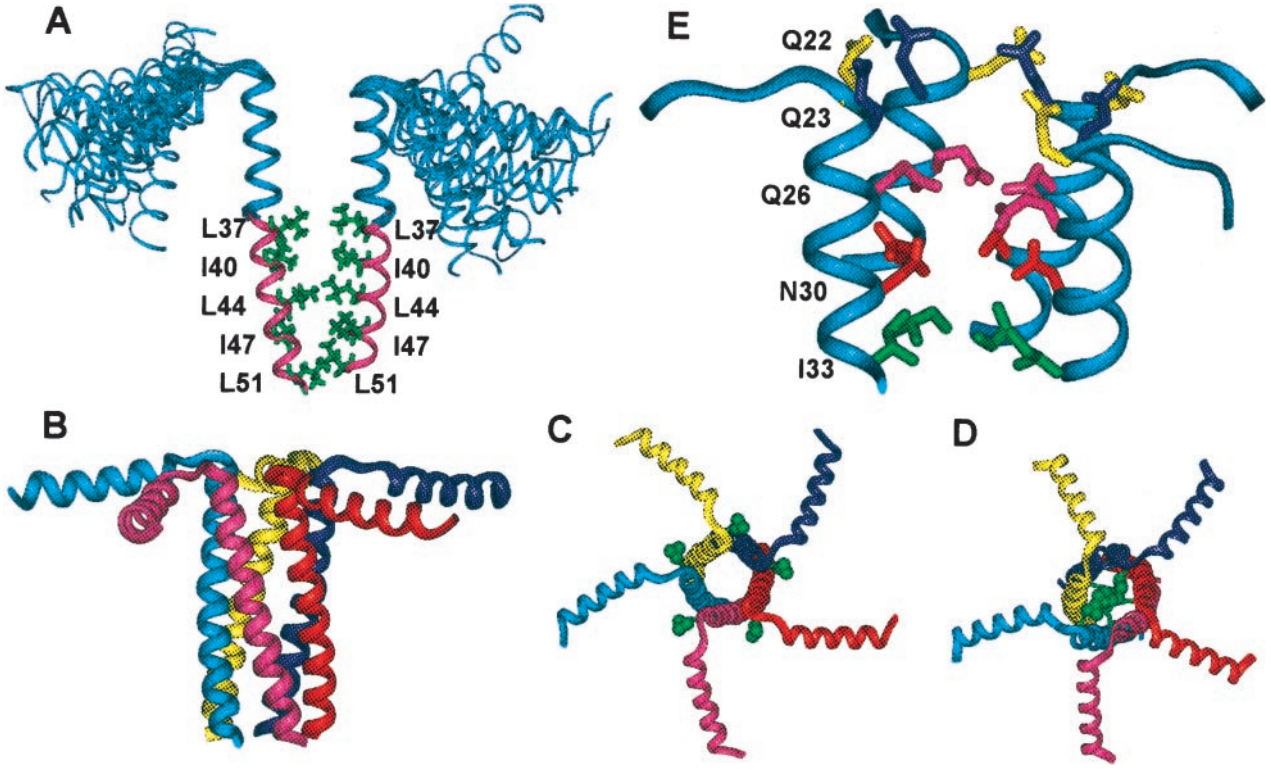

FIGURE 5 Models of PLB[1–52] pentamer obtained by connecting the structure of PLB[1–36] deduced from the NMR data of the present paper to the structures of the transmembrane PLB pentamer described in the literature. (*A*) The family of 18 NMR-derived structures of PLB[1–36] are shown as superimposed on the PLB transmembrane model stabilized by a leucine-isoleucine zipper. Only two monomers facing each other (monomers 1 and 3) are shown for clarity. Residues L37, I40, L44, I47, and L51 are shown in green. (*B* and *C*) Orthogonal views of the same PLB pentamer model as in *A*. For clarity, only the NOE-derived structure of PLB[1–36] with least violations (three violations >0.1 Å, no violations >0.2 Å) is shown. (*D*) PLB pentamer model derived by using the transmembrane model by Adams et al. (1995). In *C* and *D*, the position of the guanidino groups (the NH atoms) of Arg25 are highlighted by green balls. (*E*) The cytoplasmic part of the PLB pentamer model shown in *B* and *C*. The side chains of Gln22, Gln23, Gln26, and Asn30 are shown. Only four monomers are shown for clarity.

ical roles of the different domains of PLB is currently debated; on one side it has been shown that 1) the cytoplasmic part of PLB has a role in the inhibition of SERCA2 via an association with a well defined region of the calcium pump (Toyofuku et al., 1993, 1994a,b) and that 2) the positively charged arginines located on the cytoplasmic domain of PLB are involved in such association (Hughes et al., 1994a). However, on the other side it has been shown that also the transmembrane domain of PLB plays a role not only in the anchoring of the peptide to the membrane but also in affecting the K_{Ca} of SERCA (Sasaki et al., 1992; Kimura et al., 1996). Moreover, data were recently presented that show that PLB[26–52] in functional reconstitution of recombinant PLB with skeletal SERCA appeared to uncouple ATPase activity from calcium transport, whereas PLB[1–31] had little effect in comparison with PLB[1–52] (Reddy et al., 1995) or even that the cytoplasmic fragment PLB[2–25] is insufficient to inhibit SERCA (Jones and Field, 1993) if not acetylated at Met1 (Starling et al., 1996).

As regards other possible physiological roles of PLB, it has been proposed that the pentameric PLB may form a pore permeable to Ca^{2+} (Kovacs et al., 1988), which might possibly regulate the Ca^{2+} sequestration process, even if the pentameric structure does not appear essential for PLB inhibitory activity of SERCA2; in fact, a monomeric mutant co-expressed with SERCA does inhibit the pump (Toyofuku et al., 1994a). Recent data obtained by electron paramagnetic resonance on the PLB/lipid complexation in the membrane support a new hypothesis: namely, that the phosphorylation of PLB stabilizes the pentameric form, this being the inactive one, whereas the unphosphorylated pentamer is in rapid equilibrium with the active monomer (Cornea et al., 1997). Such a hypothesis was confirmed by the experiments of Autry and Jones on functional co-expression of canine cardiac Ca^{2+} pump and PLB (in pentamer or monomeric mutant forms) (Autry and Jones, 1997). These authors concluded that the PLB monomer is the active species in SERCA2 inhibition. Concurrently, it was also shown that the inhibition function of PLB is activated by depolymerization (Kimura et al., 1997).

Regarding the structural studies, it has been shown by CD that PLB has a secondary structure rich in α-helix (Simmerman et al., 1989; Vorherr et al., 1992). Furthermore, several groups have obtained detailed structural data by NMR for small fragments of PLB, in which higher percentages of random coil were found, due to the terminal effect. PLB[1–20] in water does not show any evidence of α-helix structure, whereas PLB[1–25] shows 60% α-helix in 50% TFE and 75% α-helix only in 100% TFE (Hubbard et al., 1994). The same fragment in water/30% TFE was shown to have α-helix structure from amino acids 1 to 17, but random coil from 18 to 25 (Mortishire-Smith et al., 1995). The structure of a PLB[1–52] point-mutated Cys41→Phe monomer in chloroform/methanol at room temperature was also resolved by NMR. In this case, however, the nature of the solvent induced a conformation where P21 did not break a 50-amino-acid-long α-helix (Maslennikov et al., 1995).

The present paper shows how PLB[1–36], which comprises the cytoplasmic domain and six amino acids of the transmembrane domain of phospholamban, assumes a conformation characterized by a high α-helical content (80%), without any evidence for residues in the β-strand. These data are in disagreement with the model proposed by Tatulian et al. (1995) based on FTIR results of phospholamban in lipid bilayer and Chou-Fasman prediction, in which the residues 22–32 form an antiparallel β-sheet. We acknowledge that the use of 30% TFE in our experiment may increment the α-helical content of the peptide. However, TFE is commonly used to stabilize α-helices in peptides that are fragments of helical regions of larger proteins (Dyson et al., 1992; Sönnichsen et al., 1992; Mortishire-Smith et al., 1995). Moreover, the number of residues with α-helical characteristics found by NMR and CD in our sample at pH 3.05 and in the presence of 30% TFE is consistent with that found earlier (40/52) by FTIR spectroscopy on a sample of PLB[1–52] reconstituted in a bilayer membrane starting from a solution at pH 7.4 (Ludlam et al., 1996). It appears thus that the titration of the carboxy terminus and of the side chains of Glu2 and Glu19 to their un-ionized form at pH 3.05, needed to maintain PLB in solution, does not cause an overall modification of the structure. It can be added that, as our strategy was to overlap and connect the carboxy terminus of our PLB[1–36] structure to the transmembrane models, it is not improper that the carboxy terminus is in its noncharged form.

The observation that the amino-terminal portion of PLB forms a less stable helix than does the carboxyl-terminal portion (see Table 2) is in agreement with the data obtained for PLB in chloroform/methanol (Maslennikov et al., 1995). Moreover, the strong upfield change of the chemical shifts of CαH (Fig. 2, $\Delta\delta$) shown for the carboxyl-terminal residues of the fragment suggests that there is no perturbation in the α-helix from residue Gln22 to the transmembrane domain.

It was shown that the structures of the fragments PLB[1–20] and PLB[9–20] in phosphorylated and unphosphorylated forms, in water and at pH 5.6, differ markedly only in the neighborhood of Ser16 and Arg14 (Quirk et al., 1996), whereas, according to other authors, the phosphorylation does induce more extensive changes in the conformation of larger amino-terminal fragments of PLB (Mortishire-Smith et al., 1995). The orientations of Ser16, Thr17, Arg9, Arg13, and Arg14 in the model proposed in the present paper are not in disagreement with the hypothesis that the phosphate group in the phosphorylated PLB will disrupt the association with SERCA by masking the positive charges of the arginine residues. The role of those positive charges in the mechanism of action of PLB seems to predominate over any other structural characteristics, as also polycations such as spermine or poly (L-Arg) do inhibit SERCA2 (Hughes et al., 1994a,b, 1995). Moreover, it has been shown that melittin (an analogue of the cytoplasmic part of phospholamban) inhibits the SERCA in skeletal SR via electrostatic cross-linking (Voss et al., 1995).

In our model, the positive charged residues in the amino-terminal helix face the carboxyl-terminal helix. This may indicate that to interact with SERCA2, PLB should assume a prolonged position (i.e., the axes of two α-helices should be nearly parallel), whereas in the bent conformation those charges would not be exposed to the ATPase but eventually to the surface charges of the phospholipid bilayer. We suggest that the apparently loose relative positioning of the two helices around the mobile central hinge could be thus a functional feature of PLB. This flexibility may explain also why, in organic solvent, PLB can assume a prolonged structure (Maslennikov et al., 1995).

Structure of the pentamer model

When comparing the two PLB[1–52] pentamer models derived alternatively from the leucine-isoleucine zipper model and from the model proposed by Adams et al., it appears clear that the latter is energetically more unfavorable due to the presence of the cluster of positive charged Arg25, whereas in the former the same residues are facing outside. Recently, a very careful re-examination of all of the experimentally measured effects of systematic single-site mutations on the phospholamban pentamer allowed to generate molecular models of the transmembrane domain (Herzyk and Hubbard, 1998), and also these data support the hypothesis that the leucine-isoleucine model is likely to be the correct one.

In addition, it can be observed that in the PLB[1–52] pentamer derived from the leucine-isoleucine zipper model the Arg25 charged side chains are facing toward the phosphorylation sites Ser16 and Thr17 of a neighboring monomer. It is thus conceivable that, after phosphorylation, the pentamer may adopt a compact conformation where Arg25 interacts with the phosphate groups of a neighboring monomer. This would be in agreement with the hypothesis that the phosphorylation of PLB stabilizes the pentamer (Cornea et al., 1997).

In the unphosphorylated form described in the present paper, however, there is not any evidence for a structure in which the amino-terminal helices assume a constrained position relative to the carboxy termini, and every monomer appears to maintain its flexibility near the turn (amino acids 18–21). This flexibility may be important in the kinetics of the monomer-pentamer association, in phosphorylation and dephosphorylation reactions, and in the association of PLB monomer and/or pentamer with SERCA2. An interesting feature in the pentamer model is the clustering of asparagines and glutamines in the cytoplasmic part of the putative ion channel. In fact, whereas the inner side of the monomers in their transmembrane segment is lined by lipophilic residues, the inner side in the cytoplasmic segment of the carboxyl-terminal α-helix is lined by polar residues.

In the COMP pentamer structure (Malashkevich et al., 1996), one of the interacting heptad positions is occupied by Gln54, the side chains of which form an internal ring interlocked by hydrogen bonds between $O^{\epsilon 1}$ and $N^{\epsilon 2}$ of neighboring residues, which would stabilize the COMP pentamer. Moreover, such a cluster is described as an ion trap, which could bind chloride anions. We found the same arrangement in the cytoplasmic part of the PLB pentamer model derived from the COMP scaffold. It could be thus hypothesized that the polar residues in the cytoplasmic part of the channel in the PLB pentamer may play a role in its function by selectively facilitating the leakage of calcium ions through the sarcoplasmic reticulum during the relaxation period of the heart cycle. However, it seems not likely that these residues could give a significant contribution to the overall stability of the pentamer, as it was shown that a single alanine mutation of the polar residues Gln22, Gln23, Gln26, and Asn30 do not destabilize it (Fujii et al., 1989; Simmerman et al., 1996).

On the other hand, the amino-terminal helix of PLB has some homologies with melittin, an amphipathic peptide that, among other properties, inhibits SERCA2 (Voss et al., 1995) and interacts with lipid bilayers forming channels (Bechinger, 1997; Kleinschmidt et al., 1997). It was recently shown that melittin is preferably oriented parallel to the phospholipids membrane (Kleinschmidt et al., 1997), in a position that the amino-terminal helix of PLB is also allowed to assume both in monomer and in pentamer form. It remains to be seen which contribution to the channel-forming characteristic of PLB is given by its amino-terminal helix.

Jorma Hermonen (Center of Biotechnology, Turku, Finland) and Ilkka Kilpeläinen (Institute of Biotechnology, Helsinki, Finland) are acknowledged for the synthesis of the PLB[1–36] peptide and for the use of the CD spectrometer, respectively.

REFERENCES

Adams, P. D., I. T. Arkin, D. M. Engelman, and A. T. Brunger. 1995. Computational searching and mutagenesis suggest a structure for the pentameric transmembrane domain of phospholamban. *Nature Struct. Biol.* 2:154–62.

Aue, W., E. Bartholdi, and R. Ernst. 1976. Two-dimensional spectroscopy: application to nuclear magnetic resonance. *J. Chem. Phys.* 64: 2229–2246.

Autry, J. M., and L. R. Jones. 1997. Functional Co-expression of the canine cardiac Ca^{2+} pump and phospholamban in *Spodoptera frugiperda* (Sf21) cells reveals new insights on ATPase regulation. *J. Biol. Chem.* 272:15872–15880.

Baxter, N., and M. Williamson. 1997. Temperature dependence of 1H chemical shifts in protein. *J. Biomol. NMR.* 9:359–369.

Bechinger, B. 1997. Structure and functions of channel-forming peptides: magainins, cecropins, melittin and alamethicin. *J. Membr. Biol.* 156: 197–211.

Bernstein, F., T. Koetzle, G. Williams, E. Meyer, M. Brice, J. Rodgers, O. Kennard, T. Shimanouchi, and M. Tasumi. 1977. *J. Mol. Biol.* 112: 535–542.

Boelens, R., T. Koning, and R. Kaptain. 1988. Determination of biomolecular structures from proton-proton NOE's using a relaxation matrix approach. *J. Mol. Struct.* 173:299–311.

Braunschweiler, L., and R. Ernst. 1983. Coherence transfer by isotropic mixing: application to proton correlation spectroscopy. *J. Magn. Reson.* 53:521–528.

Brünger, A., G. Clore, A. Gronenborn, and M. Karplus. 1986. Three-dimensional structure of proteins determined by molecular dynamics with interproton distance restraints: application to crambin. *Proc. Natl. Acad. Sci. U.S.A.* 83:3801–3805.

Chazin, W., M. Rance, and P. Wright. 1988. Complete assignment of the proton nuclear magnetic resonance spectrum of French bean plastocyanin: application of an integrated approach to spin system identification in proteins. *J. Mol. Biol.* 202:603–622.

Cornea, R. L., L. R. Jones, J. M. Autry, and D. D. Thomas. 1997. Mutation and phosphorylation change the oligomeric structure of phospholamban in lipid bilayers. *Biochemistry.* 36:2960–2967.

Dyson, H., G. Merutka, L. Waltho, R. Lerner, and P. Wright. 1992. Folding of peptide fragments comprising the complete sequence of proteins: models for initiation of protein folding. I. Myohemerythrin. *J. Mol. Biol.* 226:795–817.

Fujii, J., K. Maruyama, M. Tada, and D. H. MacLennan. 1989. Expression and site-specific mutagenesis of phospholamban: studies of residues involved in phosphorylation and pentamer formation. *J. Biol. Chem.* 264:12950–12955.

Fujii, J., A. Ueno, K. Kitano, S. Tanaka, M. Kadoma, and M. Tada. 1987. Complete complementary DNA-derived amino acid sequence of canine cardiac phospholamban. *J. Clin. Invest.* 79:301–304.

Gao, Y., B. A. Levine, D. Mornet, D. A. Slatter, and G. M. Strasburg. 1992. Interaction of calmodulin with phospholamban and caldesmon: comparative studies by 1H-NMR spectroscopy. *Biochim. Biophys. Acta.* 1160: 22–34.

Halkides, C., and A. Redfiels. 1995. The effect of ^{17}O on the relaxation of amide proton within a hydrogen bond. *J. Biomol. NMR.* 5:362–366.

Havel, T. F., G. M. Crippen, and I. D. Kuntz. 1979. Effects of distance constraints on macromolecular conformation. II. Simulation of experimental results and theoretical predictions. *Biopolymers.* 18:73–81.

Herzyk, P., and R. E. Hubbard. 1998. Using experimental information to produce a model of the transmembrane domain of the ion channel phospholamban. *Biophys. J.* 74:1203–1214.

Hicks, M., M. Shigekava, and A. Katz. 1979. Mechanism by which cyclic adenosine 3′:5′-monophosphate-dependent protein kinase stimulates calcium transport in cardiac sarcoplasmic reticulum. *Circ. Res.* 44: 383–391.

Hubbard, J. A., L. K. MacLachlan, E. Meenan, C. J. Salter, D. G. Reid, P. Lahouratate, J. Humphries, N. Stevens, D. Bell, W. A. Neville, et al. 1994. Conformation of the cytoplasmic domain of phospholamban by NMR and CD. *Mol Membr. Biol.* 11:263–269.

Hughes, G., J. M. East, and A. G. Lee. 1994a. The hydrophilic domain of phospholamban inhibits the Ca^{2+} transport step of the Ca (2+)-ATPase. *Biochem. J.* 303:511–516.

Hughes, G., Y. M. Khan, J. M. East, and A. G. Lee. 1995. Effects of polycations on Ca^{2+} binding to the Ca (2+)-ATPase. *Biochem. J.* 308:493–499.

Hughes, G., A. P. Starling, J. M. East, and A. G. Lee. 1994b. Mechanism of inhibition of the Ca (2+)-ATPase by spermine and other polycationic compounds. *Biochemistry.* 33:4745–4754.

Hughes, G., A. P. Starling, R. P. Sharma, J. M. East, and A. G. Lee. 1996. An investigation of the mechanism of inhibition of the Ca (2+)-ATPase by phospholamban. *Biochem. J.* 318:973–979.

Imagawa, T., T. Watanabe, and T. Nakamura. 1986. Subunit structure and multiple phosphorylation sites of phospholamban. *J. Biochem.* 99: 41–53.

Iwasa, T., N. Inoue, and E. Miyamoto. 1985. Identification of a calmodulin-dependent protein kinase in the cardiac cytosol, which phosphorylates phospholamban in the sarcoplasmic reticulum. *J. Biochem.* 98: 577–80.

Jackson, W., and J. Colyer. 1996. Translation of Ser16 and Thr17 phosphorylation of phospholamban into Ca (2+)-pump stimulation. *Biochem. J.* 316:201–207.

Jones, L. R., and L. J. Field. 1993. Residues 2–25 of phospholamban are insufficient to inhibit Ca^{2+} transport ATPase of cardiac sarcoplasmic reticulum. *J. Biol. Chem.* 268:11486–11488.

Karczewski, P., S. Bartel, H. Haase, and E. G. Krause. 1987. Isoproterenol induces both cAMP- and calcium-dependent phosphorylation of phospholamban in canine heart in vivo. *Biomed. Biochim. Acta.* 46: S433–S439.

Karim, C. B., J. D. Stamm, J. Karim, L. R. Jones, and D. D. Thomas. 1998. Cysteine reactivity and oligomeric structures of phospholamban and its mutants. *Biochemistry.* 37:12074–12081.

Karplus, M. 1963. Vicinal proton coupling in nuclear magnetic resonance. *J. Am. Chem. Soc.* 85:2870.

Katz, A. M., M. Tada, and M. A. Kirchberger. 1975. Control of calcium transport in the myocardium by the cyclic AMP-Protein kinase system. *Adv. Cyclic Nucleotide Res.* 5:453–472.

Kimura, Y., K. Kurzydlowski, M. Tada, and D. MacLennan. 1996. Phospholamban regulates the Ca (2+)-ATPase through intramembranes interactions. *J. Biol. Chem.* 271:21726–21731.

Kimura, Y., K. Kurzydlowski, M. Tada, and D. H. MacLennan. 1997. Phospholamban inhibitory function is activated by depolymerization. *J. Biol. Chem.* 272:15061–15064.

Kirchberger, M. A., M. Tada, and A. M. Katz. 1975. Phospholamban: a regulatory protein of the cardiac sarcoplasmic reticulum. *Rec. Adv. Stud. Cardiac Struct. Metab.* 5:103–115.

Kleinschmidt, J. H., J. E. Mahaney, D. D. Thomas, and D. Marsh. 1997. Interaction of bee venom melittin with zwitterionic and negatively charged phospholipid bilayers: a spin-label electron spin resonance study. *Biophys. J.* 72:767–778.

Kovacs, R. J., M. T. Nelson, H. K. Simmerman, and L. R. Jones. 1988. Phospholamban forms Ca^{2+}-selective channels in lipid bilayers. *J. Biol. Chem.* 263:18364–18368.

Kumar, A., R. Ernst, and K. Wüthrich. 1980. A two-dimensional nuclear Overhauser enhancement (2D NOE) experiment for the elucidation of complete proton-proton cross-relaxation networks in biological macromolecules. *Biochem. Biophys. Res. Commun.* 95:1–6.

Laskowski, R. A., J. A. C. Rullmann, M. W. MacArthur, R. Kaptein, and J. M. Thornton. 1996. AQUA and PROCHECK-NMR: programs for checking the quality of protein structures solved by NMR. *J. Biomol. NMR.* 8:477–486.

Ludlam, C., I. Arkin, X. Liu, M. Rothman, P. Rath, S. Aimoto, S. Smith, D. Engelman, and K. Rothschild. 1996. Fourier transform infrared spectroscopy and site-directed isotope labeling as a probe of local secondary structure in the transmembrane domain of phospholamban. *Biophys. J.* 70:1728–1736.

Malashkevich, V., R. Kammerer, V. Efimov, T. Schulthess, and J. Engel. 1996. The crystal structure of a five-stranded coiled coil in COMP: a prototype ion channel? *Science.* 274:761–765.

Marion, D., M. Ikura, and A. Bax. 1989a. Improved solvent suppression in one- and two-dimensional NMR spectra by convolution of time-domain data. *J. Magn. Res.* 84:425–430.

Marion, D., M. Ikura, R. Tschudin, and A. Bax. 1989b. Rapid recording of 2D NMR spectra without phase cycling: application to the study of hydrogen exchange in proteins. *J. Magn. Reson.* 85:393–399.

Maslennikov, I. V., A. G. Sobol, J. Anagli, P. James, T. Vorherr, A. S. Arseniev, and E. Carafoli. 1995. The secondary structure of phospholamban: a two-dimensional NMR study. *Biochem. Biophys. Res. Commun.* 217:1200–1207.

McIntyre, L., and R. Freeman. 1992. Accurate measurements of coupling constants by *J* doubling. *J. Magn. Reson.* 96:425–431.

Meyer, M., W. Schillinger, B. Pieske, C. Holubarsch, C. Heilmann, H. Posival, G. Kuwajima, K. Mikoshiba, H. Just, G. Hasenfuss, et al. 1995. Alterations of sarcoplasmic reticulum proteins in failing human dilated cardiomyopathy. *Circulation.* 92:778–784.

Mortishire-Smith, R. J., S. M. Pitzenberger, C. J. Burke, C. R. Middaugh, V. M. Garsky, and R. G. Johnson. 1995. Solution structure of the cytoplasmic domain of phospholamban: phosphorylation leads to a local perturbation in secondary structure. *Biochemistry.* 34:7603–7613.

Quirk, P., V. Patchell, J. Colyer, G. Drago, and Y. Gao. 1996. Conformational effects of serine phosphorylation in phospholamban peptides. *Eur. J. Biochem.* 236:85–91.

Reddy, L. G., L. R. Jones, S. E. Cala, J. J. O'Brian, S. A. Tatulian, and D. L. Stokes. 1995. Functional reconstitution of recombinant phospholamban with rabbit skeletal Ca (2+)-ATPase. *J. Biol. Chem.* 270: 9390–9397.

Rothemund, S., H. Weisshoff, M. Beyermann, E. Krause, M. Bienert, C. Muegge, B. Syker, and F. Soennichsen. 1996. Temperature coefficient of amide proton NMR resonance frequencies in trifluoroethanol: a

monitor of intramolecular hydrogen bonds in helical peptides? *J. Biomol. NMR.* 8:93–97.

Sasaki, T., M. Inui, Y. Kimura, T. Kuzuya, and M. Tada. 1992. Molecular mechanism of regulation of Ca^{2+} pump ATPase by phospholamban in cardiac sarcoplasmic reticulum: effects of synthetic phospholamban peptides on Ca^{2+} pump ATPase. *J. Biol. Chem.* 267:1674–1679.

Simmerman, H. K. B., J. H. Collins, J. L. Theibert, A. D. Wegener, and L. R. Jones. 1986. Sequence analysis of phospholamban:. Identification of phosphorylation sites and two major structural domains. *J. Biol. Chem.* 261:13333–13341.

Simmerman, H. K. B., Y. M. Kobayashi, J. M. Autry, and L. R. Jones. 1996. A leucine zipper stabilizes the pentameric membrane domain of phospholamban and forms a coiled-coil pore structure. *J. Biol. Chem.* 271:5941–5946.

Simmerman, H. K. B., D. E. Lovelace, and L. R. Jones. 1989. Secondary structure of detergent-solubilized phospholamban, a phosphorylatable, oligomeric protein of cardiac sarcoplasmic reticulum. *Biochim. Biophys. Acta.* 997:322–329.

Starling, A., R. Sharma, J. East, and A. Lee. 1996. The effect of N-terminal acetylation on Ca^{2+}-ATPase inhibition by phospholamban. *Biochem. Biophys. Res. Commun.* 226:352–355.

Stopar, D., R. Spruijt, C. Wolfs, and M. Hemminga. 1996. Local dynamics of the M13 major coat protein in different membrane-mimicking systems. *Biochemistry.* 35:5467–5473.

Sönnichsen, F., J. Van Eyk, R. Hodges, and B. Sykes. 1992. Effect of trifluoroethanol on protein secondary structure: an NMR and CD study using a synthetic actin peptide. *Biochemistry.* 31:8790–8798.

Tada, M., and M. Kadoma. 1989. Regulation of the Ca^{2+} pump ATPase by cAMP-dependent phosphorylation of phospholamban. *Bioessays.* 10: 157–163.

Tatulian, S. A., L. R. Jones, L. G. Reddy, D. L. Stokes, and L. K. Tamm. 1995. Secondary structure and orientation of phospholamban reconstituted in supported bilayers from polarized attenuated total reflection FTIR spectroscopy. *Biochemistry.* 34:4448–4456.

Terzi, E., L. Poteur, and E. Trifilieff. 1992. Evidence for a phosphorylation-induced conformational change in phospholamban cytoplasmic domain by CD analysis. *FEBS Lett.* 309:413–416.

Toyofuku, T., K. Kurzydlowski, M. Tada, and D. H. MacLennan. 1993. Identification of regions in the Ca (2+)-ATPase of sarcoplasmic reticulum that affect functional association with phospholamban. *J. Biol. Chem.* 268:2809–2815.

Toyofuku, T., K. Kurzydlowski, M. Tada, and D. H. MacLennan. 1994a. Amino acids Glu2 to Ile18 in the cytoplasmic domain of phospholamban are essential for functional association with the Ca (2+)-ATPase of sarcoplasmic reticulum. *J. Biol. Chem.* 269:3088–3094.

Toyofuku, T., K. Kurzydlowski, M. Tada, and D. H. MacLennan. 1994b. Amino acids Lys-Asp-Asp-Lys-Pro-Val402 in the Ca (2+)-ATPase of cardiac sarcoplasmic reticulum are critical for functional association with phospholamban. *J. Biol. Chem.* 269:22929–22932.

Vorherr, T., M. Chiesi, R. Schwaller, and E. Carafoli. 1992. Regulation of the calcium ion pump of sarcoplasmic reticulum: reversible inhibition by phospholamban and by the calmodulin binding domain of the plasma membrane calcium ion pump. *Biochemistry.* 31:371–376.

Vorherr, T., A. Wrzosek, M. Chiesi, and E. Carafoli. 1993. Total synthesis and functional properties of the membrane-intrinsic protein phospholamban. *Protein Sci.* 2:339–347.

Voss, J. C., J. E. Mahaney, and D. D. Thomas. 1995. Mechanism of Ca-ATPase inhibition by melittin in skeletal sarcoplasmic reticulum. *Biochemistry.* 34:930–939.

Wishart, D. S., B. D. Sykes, and F. M. Richards. 1991a. Relationship between nuclear magnetic resonance chemical shift and protein secondary structure. *J. Mol. Biol.* 223:331–333.

Wishart, D. S., B. D. Sykes, and F. M. Richards. 1991b. Simple techniques for the quantification of protein secondary structure by 1H NMR spectroscopy. *FEBS.* 293:72–80.

Wishart, D. S., B. D. Sykes, and F. M. Richards. 1992. The chemical shift index: a fast and simple method for the assignment of protein secondary structure through NMR spectroscopy. *Biochemistry.* 31:1647–1651.

Wüthrich, K. 1986. NMR of Proteins and Nucleic Acids. John Wiley and Sons, New York.

Wüthrich, K., M. Billetter, and W. Braun. 1983. Pseudostructures for the 20 common amino acids for use in studies of protein conformations by measurements of intramolecular proton-proton distance constraints with nuclear magnetic resonance. *J. Mol. Biol.* 169: 949–961.

Yeagle, P., J. Aldelfer, and A. Albert. 1997. Three-dimensional structure of the cytoplasmic face of the G protein receptor rhodopsin. *Biochemistry.* 36:9649–9654.